Frequency-Induced Bulk Magnetic Domain-Wall Freezing Visualized by Neutron Dark-Field Imaging

B. Betz,[1,2] P. Rauscher,[3] R. P. Harti,[1] R. Schäfer,[4] H. Van Swygenhoven,[2,5] A. Kaestner,[1] J. Hovind,[1] E. Lehmann,[1] and C. Grünzweig[1]

[1]*Paul Scherrer Institut, LNS, Neutron imaging and Activation Group, CH-5232 Villigen, Switzerland*
[2]*Ecole polytechnique fédérale de Lausanne, NXMM, IMX, CH-1015 Lausanne, Switzerland*
[3]*Fraunhofer IWS Dresden, Laser Ablation and Cutting, D-01069 Dresden, Germany*
[4]*Leibniz Institute for Solid State and Materials Research (IFW) Dresden, D-01069 Dresden, Germany, and Institute for Materials Science, TU Dresden, D-01069 Dresden, Germany*
[5]*Paul Scherrer Institut, Photons for Engineering and Manufacturing, CH-5232 Villigen, Switzerland*

(Received 29 December 2015; revised manuscript received 3 May 2016; published 30 August 2016)

We use neutron dark-field imaging to visualize and interpret the response of bulk magnetic domain walls to static and dynamic magnetic excitations in (110)-Goss textured iron silicon high-permeability steel alloy. We investigate the domain-wall motion under the influence of an external alternating sinusoidal magnetic field. In particular, we perform scans combining varying levels of dc_{offset} (0–30 A/m), oscillation amplitude A_{ac} (0–1500 A/m), and frequency f_{ac} ((0–200 Hz). By increasing amplitude A_{ac} while maintaining constant values of dc_{offset} and f_{ac}, we record the transition from a frozen domain-wall structure to a mobile one. Vice versa, increasing f_{ac} while keeping A_{ac} and dc_{offset} constant led to the reverse transition from a mobile domain-wall structure into a frozen one. We show that varying both A_{ac} and f_{ac} shifts the position of the transition region. Furthermore, we demonstrate that higher frequencies require higher oscillation amplitudes to overcome the freezing phenomena. The fundamental determination and understanding of the frequency-induced freezing process in high-permeability steel alloys is of high interest to the further development of descriptive models for bulk macromagnetic phenomena. Likewise, the efficiency of transformers can be improved based on our results, since these alloys are used as transformer core material.

DOI: 10.1103/PhysRevApplied.6.024024

I. INTRODUCTION

Transformers are electromagnetic devices that transfer electrical energy through electromagnetic induction. The cores of transformers are primarily made of high-permeability silicon steel alloys, and most of this steel is Goss-oriented [1] electrical steel because the anisotropic magnetic properties are in alignment with the rolling direction, providing an optimal magnetic flux path [2–4]. In a transformer, an alternating voltage is transferred into a second voltage; therefore, transformer cores are strained by an alternating magnetic field. The properties of a transformer, such as losses and the degree of efficiency, are determined by the behavior of the magnetic domain structure inside the core material. The global magnetic properties of Goss-oriented steels, though, are predominantly characterized using inductive B-H-hysteresis measurements [5]. This experimental technique does not reveal the underlying domain response. Investigations of the surface domain structure are predominantly performed using Kerr microscopy [6]. Unfortunately, this technique is not able to investigate volume domain structures; only an indirect interpretation of the volume domain response is possible while studying the surface effects.

We conduct neutron-grating interferometry experiments [7–9] to study the response of the bulk magnetic domain-wall structure to an alternating sinusoidal magnetic excitation. The visualization of magnetic domain structures using the neutron dark-field image (DFI) in two [10–13] and in three [13] dimensions has been reported previously, however, only under the influence of static magnetic fields. We report in this article on the visualization of the dynamic volume domain response to externally applied alternating magnetic fields. Hereby, we could identify the transition regions between frequency-induced domain-wall freezing and amplitude-induced domain-wall mobilization.

II. EXPERIMENTAL SETUP AND DATA-ACQUISITION MATRIX

The experiments are carried out at the Swiss Spallation Neutron Source using the cold neutron imaging facility ICON [14] at Paul Scherrer Institut. The neutron-grating interferometry setup used for the alternating magnetic field measurements is shown in Fig. 1. The use of the source grating G_0 acting as a periodic line source, followed by the phase grating G_1 at a distance l, and the analyzer grating G_2 at the Talbot distance d_T behind G_1, allows for the spatially resolved detection of the sample's scattering properties [10–13]. The interaction of the magnetic moment of a neutron with the magnetic induction of ferromagnetic domains results in a local scattering of the incoming neutron beam, which is visualized in the corresponding

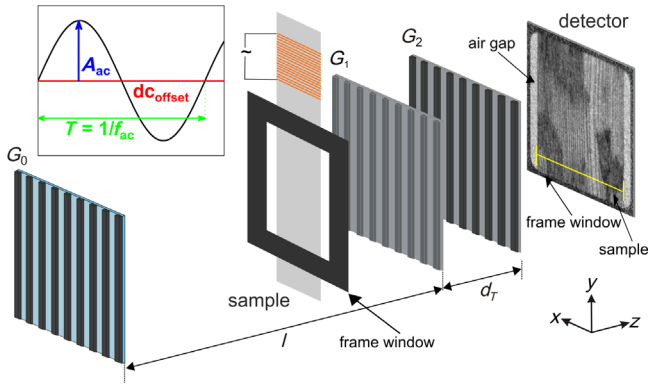

FIG. 1. Schematic of the neutron-grating interferometer for the investigation of the bulk magnetic domain structure under the influence of externally applied alternating magnetic fields with varying parameters dc_{offset}, A_{ac}, and f_{ac} as explained in the inset. The source grating G_0 is placed at a distance l from the phase grating G_1, which is followed by the analyzer grating G_2 at the Talbot distance d_T. The sample is mounted in the magnetization frame and placed as close as possible in front of G_1. The images are recorded using a scintillator-based neutron imaging detection system.

DFI. Further details about the contrast formation can be found in Refs. [10–13]. The DFIs are recorded by a conventional scintillator (100-μm-thick ^{6}LiF/ZnS) based detection system using a digital camera (Andor NEO sCMOS, 2160×2560 pixels; pixel size 6.5 μm) placed behind G_2. The effective spatial resolution in our measurements is 70 μm and is determined by intrinsic blurring of the scintillation screen [15] and penumbra blurring caused by the sample-to-detector distance of 3 cm. The exposure time of a single DFI is in the range of 25 min. Thus, it is not possible to visualize a domain wall in motion in real time under conditions of alternating magnetic fields, and the recorded DFIs correspond to a time-averaged domain-wall position at steady state for pairs of A and f.

The steel sample used in our measurements is a highly anisotropic Goss-oriented iron alloy sheet with approximately 3% silicon coated by a fosterite and phosphate layer, a form of electric steel that is widely used as transformer core material. The sample used for the investigations is in accordance with the standard grade EN 10107: M 100-30 P (Thyssen-Krupp powerCore H, Grade: H 100-30, Core losses at 1.7 T and 50 Hz: 1.00 W/kg), and has a width of 30 mm, a length of 300 mm, and a thickness of 300 μm. The sheet is inserted in a magnetization frame which is mounted directly in front of the phase grating. The field of view is 35 mm $\times$ 35 mm limited by the frame window. Alternating magnetic fields are induced by a coil which is supplied with current from an ac power supply [KEPCO BOP100-4ML]. The inset schematically depicts the applied magnetic field parameters. A sinusoidal excitation is used with the following parameters, which could be individually varied. The offset of the oscillation dc_{offset} (red) is a constant current. The amplitude of the sinusoidal oscillation A_{ac} (blue) and the period T or the frequency f_{ac} (green) of the oscillation are superimposed onto this offset. By way of example, a DFI of the sample is shown on the detector. The air gap and the frame window are also visible.

The behavior of the bulk magnetic domain structure to dynamic investigation under the influence of alternating magnetic fields differs from static investigations using dc fields in several ways. The alternating, periodical excitation of domain-wall movement induces eddy currents which act opposite to the externally applied field and weaken the driving force [16,17]. With increasing frequencies, the wall velocity needs to also increase, which further enhances the eddy-current damping. Altogether, this decreases the domain-wall mobility.

We investigate the magnetic domain response to variation in three parameters to examine the frequency-dependent domain-wall mobility. The parameters varied are dc_{offset}, the oscillation amplitude A_{ac}, and the frequency f_{ac}. The corresponding data-acquisition matrix is shown in Fig. 2. Each sphere corresponds to a single DFI measurement. The first investigation is a scan of the dc_{offset} parameter without any oscillation applied ($A_{ac} = 0$ A/m; $f_{ac} = 0$ Hz). This trajectory is marked by the red spheres in Fig. 2 and the corresponding results are presented in Fig. 3. This scan reveals the quasistatic magnetization behavior. The dc_{offset} is fixed to 4.5 A/m for the remaining investigations, placing the results in the red plane as schematically depicted in Fig. 2. To represent the amplitude-dependent magnetization behavior, a so-called "isofrequency" scan is performed with a fixed

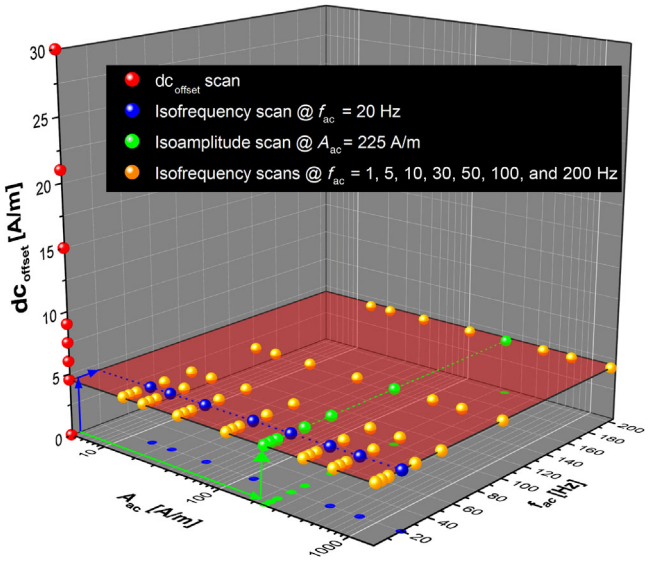

FIG. 2. Data-acquisition matrix for the dc_{offset},the oscillation amplitude A_{ac}, and frequency f_{ac} of the alternating sinusoidal magnetic field. Each sphere represents DFI measurement. The red spheres mark the dc_{offset} scan, blue spheres represent the isofrequency scan at a fixed frequency of $f_{ac} = 20$ Hz with increasing oscillation amplitude, green spheres illustrate the isoamplitude scan at a fixed amplitude $A_{ac} = 225$ A/m with increasing frequency, and orange spheres indicate the completing isofrequency scans.

frequency of $f_{ac} = 20$ Hz, while the amplitude A_{ac} is stepwise increased from 15 A/m up to 1500 A/m. This scan is illustrated by the blue spheres in Fig. 2 and the corresponding DFIs are shown in Fig. 4. To depict the frequency-dependent magnetization behavior, an analogous "isoamplitude" scan is conducted, where the amplitude is fixed at $A_{ac} = 225$ A/m and the frequency f_{ac} is increased from 1 Hz up to 200 Hz. This scan is illustrated by the green spheres in Fig. 2 and the corresponding DFIs are presented in Fig. 5. To complete the data-acquisition matrix, the remaining data points are covered by consecutively recording isofrequency scans at $f_{ac} = 1$, 5, 10, 20, 30, 50, 100, and 200 Hz, with the amplitude A_{ac} incrementally increased from 15 A/m up to 1500 A/m as in the isofrequency scan. These data points are shown by the orange spheres in Fig. 2, while the corresponding DFIs are shown in Fig. 6.

III. EXPERIMENTAL RESULTS

A. dc_{offset} scan

The DFI results of the dc_{offset} scan (denoted by the red spheres in Fig. 2) are shown in Fig. 3. The DFI at 0 A/m, without magnetic field applied, shows a pronounced contrast with dedicated features. The contrast in the DFI is generated due to the scattering of neutrons at the magnetic domain walls. This scattering leads to a loss of coherence and consequently to a degraded DFI signal [10–13]. The black vertical lines in the DFI depict an elongated magnetic volume domain structure, while the black lines themselves represent the domain walls. These individual domain walls can be made visible because the domain width is larger than the detector resolution. The sample is mounted in such a way that the crystallographic [001] direction is aligned parallel to the grating lines. Accordingly, the magnetization of the 180° basic domain points in a vertical direction [16].

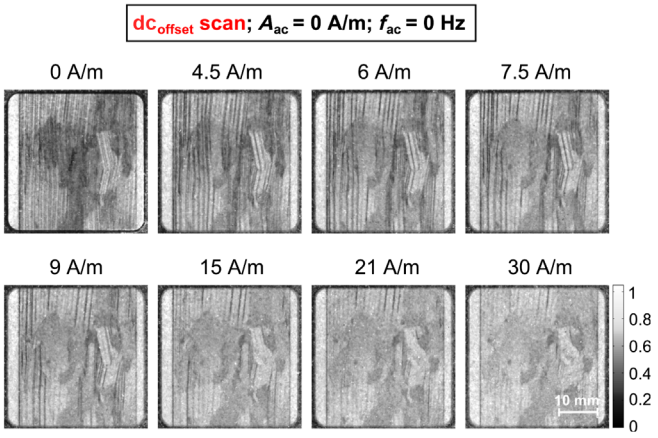

FIG. 3. Static visualization of the bulk domain-wall structure and response to an applied dc_{offset}. DFIs for increasing field values from $dc_{offset} = 0$ to 30 A/m are shown (red spheres in Fig. 2). Large vertically elongated domains are depicted by black lines, representing the domain walls. Misoriented grains appear as dark areas.

The magnetic field is applied in this direction for subsequent investigations. In addition to the basic domain structure, centimeter-sized areas with a decreased DFI value can be observed. These areas indicate grains with a crystallographic misorientation (i.e., out-of-plane misalignment of the almost surface-parallel [001] easy axis by some degrees), leading to the generation of supplementary domains [16] that are smaller to the detector resolution. Consequently, a decreased average DFI signal is interpreted as a higher relative density of domain walls.

Applying a magnetic field of $dc_{offset} = 4.5$ A/m leads to the cancellation of several volume domain walls, which are visible in the DFI as an increased domain-wall spacing ranging from several hundred of microns up to several mm. Magnetic domains with a magnetization pointing in the direction of the applied magnetic field need to grow at the cost of those pointing in the opposite direction. This is due to the magnetic flux that needs to be transported along the lamination. The pinning of these basic domain walls and their (possibly) abrupt unsnapping (Barkhausen jumps [18]) during magnetization, in combination with the exposure time of a single DFI, causes the instantaneous jumps of the domain walls to appear as continuous changes in the domain structure. The contrast of misoriented grains changes because of simultaneous changes in the underlying basic domain structure, while the contrast originating from the supplementary domains remains constant. Further increasing the dc_{offset} to 6, 7.5, 9, 15, and 21 A/m, consecutively, leads to additional basic domain walls vanishing, while they either end at grain boundaries or penetrate misoriented grains to ensure flux continuity, seen especially in the DFI at $dc_{offset} = 4.5$ A/m. If they penetrate the misoriented grains, the basic domains build an underlying structure in addition to the supplementary domains. These findings are also supported by Shin *et al.* [19]. For an applied field of dc_{offset} 30 A/m only a few basic domain walls can be found, whereas the misoriented grains remain visible due to the supplementary domains being still present at higher fields.

In the following sections, we investigate the response of domain structures to external magnetic sinusoidal excitation that is superimposed on a dc_{offset} value of 4.5 A/m. We investigate the frequency- and amplitude-dependent freezing and mobilization behavior of bulk magnetic domain structures in detail.

B. Isofrequency scan

We first investigate the amplitude-dependent behavior of the bulk domain structure. We apply a sinusoidal oscillation with a frequency of $f_{ac} = 20$ Hz in superposition to the dc_{offset} of 4.5 A/m. The results are shown in Fig. 4. In all DFIs the contrast provided by the supplementary domains in the misoriented grains remains constant and is independent from A_{ac}. What we do see is a change in the basic domain walls. In the DFI with an amplitude of $A_{ac} = 15$ A/m, basic domains are visible as are the

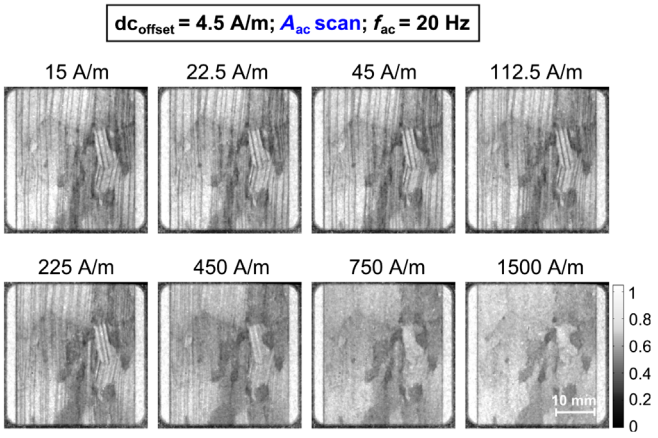

FIG. 4. DFIs of the isofrequency scan (blue spheres in Fig. 2) at $f_{ac} = 20$ Hz and $dc_{offset} = 4.5$ A/m. Stationary domain walls are observed until the amplitude in the transition region ($A_{ac} = 450$ A/m) starts to excite the domain walls, causing them to tremble. A further increase in amplitude leads to a mobilization of the basic domain walls, seen as a gray veil that represents the average position of the domain walls during the scan.

supplementary domains, by an average decreased DFI signal, in the misoriented grains. The sharp image of the discrete basic domains indicates that the basic domain walls are stationary. When we compare the DFI with $A_{ac} = 15$ A/m in Fig. 4 to the DFI with a $dc_{offset} = 15$ A/m in Fig. 3, we see two different magnetic states. In the dc_{offset} version, the most basic domain walls have already vanished. However, in the A_{ac} version many stationary, at least within our resolution, domain walls are, surprisingly, observed. Increasing the amplitude A_{ac} up to 22.5, 45, and 112.5 A/m, respectively, does not induce significant changes in the domain-wall structure, as can be seen in the corresponding DFIs. The domain structure remains frozen, meaning the domain walls do not move. In the DFI with an amplitude of $A_{ac} = 225$ A/m, the basic domain walls appear blurred. This is interpreted as a trembling of the domain walls around their initial position. This trembling-based blurring increases with increasing amplitude as seen in the DFI with $A_{ac} = 450$ A/m, until the domain structure starts to unfreeze. Until here, we observe a refinement of the basic domain structure visible by decreasing domain widths with extreme values of several mm down to several hundred microns. Further increasing the applied amplitude A_{ac} to 750 and 1500 A/m, respectively, the basic domains are completely converted into a gray veil over the whole sample. This veil represents the average position of the domain walls as they move across the sample during the multitude of alternating field cycles. The basic domain structure is finally entirely mobilized at these amplitudes.

The transition from frozen to mobilized basic domain walls is not instantaneous. Small amplitudes maintain stationary domain structures. The domain walls start to tremble under moderate amplitudes with the distance traveled increasing at higher amplitudes. The distance traveled increases until neighboring domain walls intersect. The intersection of domain walls is depicted as a gray veil in the DFIs due to the long exposure time. The steady process of unfreezing leads to a transition region between 225 and 750 A/m instead of a sharp transition point.

The transition from the frozen to mobilized basic domain structure is caused by eddy-current damping phenomena. The eddy-current damping D is proportional to the square of the velocity v of domain walls v^2, which is proportional to the square of the exciting frequency f_{ac}^2 [20]:

$$D \sim v^2 \sim f_{ac}^2. \tag{1}$$

At a fixed frequency f_{ac}, the amplitude A_{ac} needs to overcome a threshold value to energetically compensate for the frequency-induced eddy-current damping. Note that the DFI in Fig. 3 with $dc_{offset} = 30$ A/m and the DFI in Fig. 4 with an A_{ac} of 1500 A/m look rather similar. However, the origins of the contrast in both images fundamentally differ. The contrast in the dc_{offset} DFI represents only one point in the hysteresis curve. In this case, a net magnetic flux can be transported across the sample, due to the domain structure arrangement. Therefore, domain walls are effectively expelled from the sample. In the case of an alternating field, the domain walls are not completely expelled from the sample, but are invisible due to their motion.

In the following section, we discuss the magnetic domain structure under variable oscillation frequencies f_{ac}, while the amplitude A_{ac} and the dc_{offset} are kept constant.

C. Isoamplitude scan

The bulk magnetic domain behavior is expected to depend not only on the applied amplitude but also on

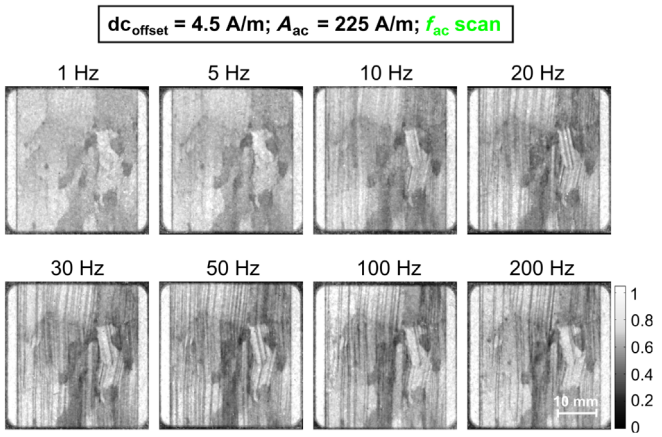

FIG. 5. Frequency-induced bulk magnetic domain-wall freezing. DFIs of an isoamplitude-scan (green spheres in Fig. 2) at a $dc_{offset} = 4.5$ A/m and an $A_{ac} = 225$ A/m. At low frequencies, domain walls are mobilized. The transition into a frozen domain structure is observed between 5–10 Hz. For higher frequencies, the domain walls stay frozen and no significant changes in the DFIs are recorded.

the frequency of the exciting oscillation [17,20]. It is known from hysteresis loop measurements, that eddy-current damping in iron-silicon alloys is especially dependent on the applied frequency. We investigate the frequency-dependent domain freezing process by conducting a series of measurements using a fixed amplitude of $A_{ac} = 225$ A/m superimposed on a $dc_{offset} = 4.5$ A/m, while the frequency is incrementally increased from 1 to

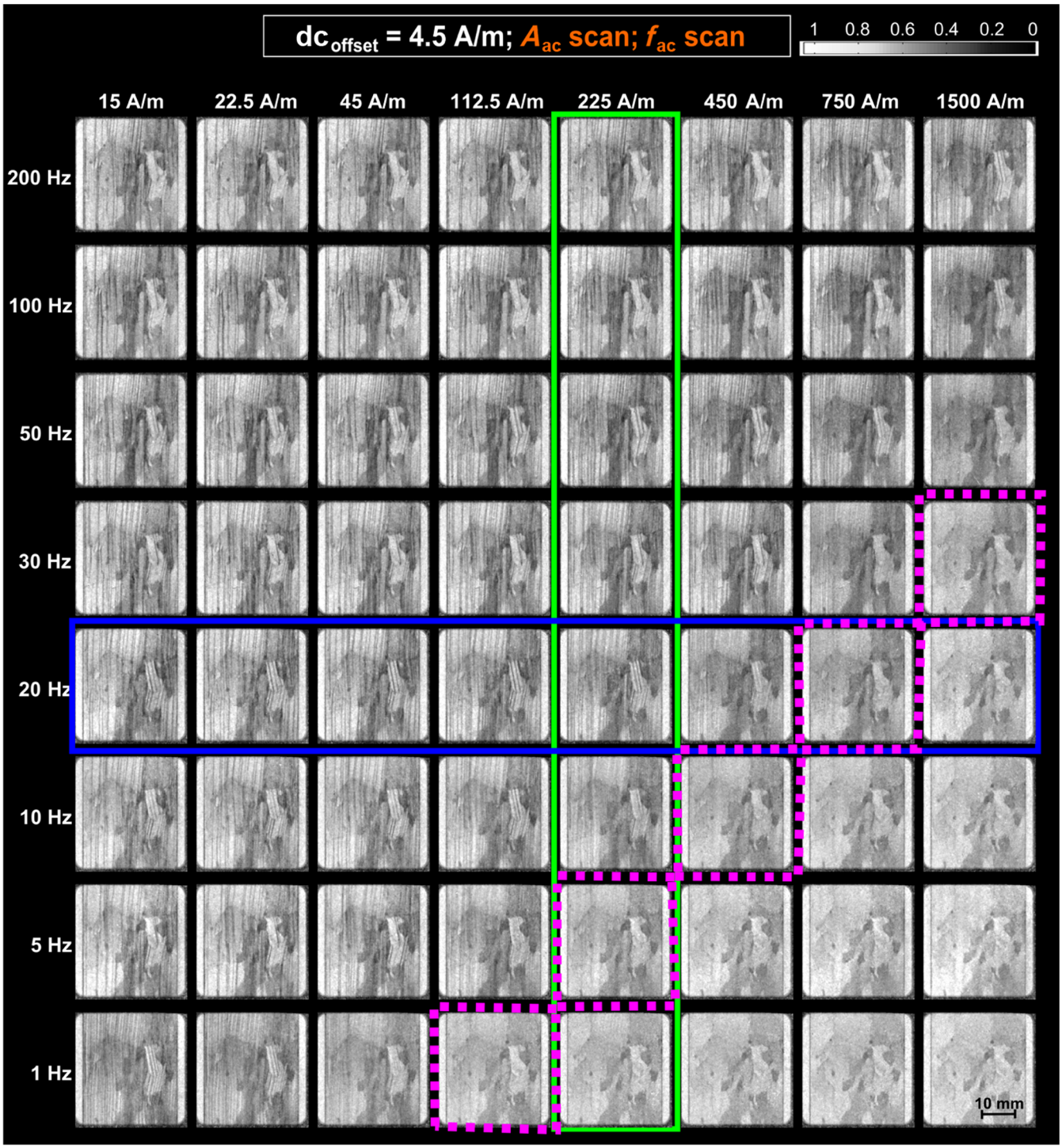

FIG. 6. Data-acquisition matrix showing the amplitude- and frequency-dependent shift in the transition between frozen and mobilized basic domain-wall structures. In the upper-left part of the figure with high frequencies and small amplitudes, frozen domain walls are observed. In the bottom-right part of the figure with large amplitudes and small frequencies, mobilized domain walls are seen. Representative isofrequency and isoamplitude scans are marked by the blue and green boxes, respectively. The DFIs showing the transition points are marked by purple dashed boxes.

200 Hz. We consequently call this an "isoamplitude scan". The DFI results are shown in Fig. 5.

Interestingly, the DFIs for increasing frequencies f_{ac} reveal an inverted freezing and mobilization behavior to that found for increasing amplitudes A_{ac} in Fig. 4. The isofrequency scan in Fig. 4 shows the domain-wall mobilization, whereas in the isoamplitude scan in Fig. 5 the frequency-induced freezing is visualized. No basic domain walls are visible in Fig. 5 in the beginning with a frequency of 1 Hz. The applied amplitude in combination with low frequencies of 1 and 5 Hz leads to the basic domain walls being mobilized, resulting in a gray veil as explained above. In the DFI with $f_{ac} = 10$ Hz the basic domain walls start to become visible; the domain walls are visualized as blurred lines as a consequence of their trembling. In the transition region between 5 and 10 Hz, the basic domain-wall structure freezes and becomes stationary. Even for higher frequencies such as 20, 30, 50, 100, and 200 Hz, the basic domain walls remain frozen and no significant changes in the DFIs are recorded except a trend of increasing the basic domain width for several hundred microns up to mm. The transformation into a frozen domain-wall structure can likewise be explained by the eddy-current damping phenomena. An increase in frequency f_{ac} according to Eq. (1) leads to an increased domain-wall velocity v, which results in larger eddy-current damping.

Hence, a magnetic field amplitude of $A_{ac} = 225$ A/m is large enough to compensate energetically for the eddy-current damping related to the skin effect at a frequency of 5 Hz and the domain walls are mobile. In contrast, at 10 Hz the excitation amplitude is no longer large enough to compensate for the damping, which is proportional to the frequency squared, and the domain walls are frozen. In contrast to the basic domain structure, the supplementary domain structure in the misoriented grains reveals no frequency-dependent behavior.

The results so far show both an amplitude- and frequency-dependent transition region between frozen and mobilized basic domain-wall structures. In the following section, we further study the interplay of these two parameters with respect to the induced freezing phenomena of the basic domain structures.

D. Frequency-dependent transition regions

To complete the data-acquisition matrix, we perform additional isofrequency scans at 1, 5, 10, 30, 50, 100, and 200 Hz, as indicated by the orange spheres in Fig. 2. The corresponding DFI results can be found in Fig. 6. The data of the isofrequency scan from Fig. 4 are marked by a blue box and the data for the isoamplitude scan shown in Fig. 5 by a green box, respectively. For small amplitudes A_{ac} and high frequencies f_{ac} (upper-left part of the data-acquisition matrix), the basic domain walls are found in a frozen state, whereas for high amplitudes and small frequencies the basic domain walls are found in a mobilized state (bottom-right part of the data-acquisition matrix). Similar to the isofrequency scan at 20 Hz (blue box), no significant changes in the basic domain structure are observed in the isofrequency scans from 1–200 Hz until the particular mobilization (unfreezing) of the domain structure occurs. These transitions are marked by the purple dashed boxes. The particular transition regions are found to be frequency dependent. Higher frequencies need higher excitation amplitudes to overcome freezing. Since the eddy-current damping increases with increasing frequencies, the amplitude to compensate for these needs to be concordantly increased. At a frequency of 50 Hz and an amplitude of 1500 A/m, we barely reach the transition region. This is due to the limitations of our sample environment, which does not allow for the application of higher field values. For larger frequencies of 100 and 200 Hz, we are not able to apply sufficiently large amplitudes to mobilize the basic domain walls. Despite these limitations, we can clearly see the trend that larger amplitudes are needed to transform frozen basic domain walls into mobilized domain-wall structures at increased frequencies.

IV. CONCLUSION AND OUTLOOK

In this article, we investigate the bulk magnetic domain response of an iron silicon alloy under varying frequencies and amplitudes of a sinusoidal magnetic field oscillation given a constant dc offset value. We apply the neutron-grating interferometer technique, which provides a time-averaged position for the domain wall in the neutron dark-field image. We are able to identify transitions of the basic domain structure from a frozen into a mobilized state and vice versa. The isoamplitude scan shows that the freezing of the domain structure is induced by increasing the excitation frequency. In contrast, the isofrequency scan reveals that increasing the excitation amplitude leads to a mobilization of the domain structure. We can identify a shift of the transition region towards higher amplitudes for increasing frequencies by studying in detail the interplay between the frequency and amplitude of the magnetic excitation. Thus, we can visualize the frequency-induced freezing phenomena of bulk magnetic domain walls. There is a lack of spatially explicit alternative techniques to directly investigate bulk magnetic structures; however, our experimental findings support existing theoretical descriptions of the bulk magnetic domain behavior. The basic understanding of the frequency-induced freezing process in high-permeability steel alloys is of high interest to the further development of descriptive models for bulk macromagnetic phenomena. So far, all theoretical existing domain models for electrical steel laminations are based on surface domain observations, combined with domain-theoretical arguments. An experimental proof of the model does not exist, and here our DFI findings make a contribution.

Likewise, the performance and efficiency of transformers can be improved based on our results since these alloys are predominantly used as transformer core material. Future experiments using a time-resolved detector setup will provide a more detailed insight into the dynamic magnetic domain-wall behavior, especially in the transition regions.

[1] N. P. Goss, Electrical sheet and method and apparatus for its manufacture and test, U.S. Patent No. 1,965,559 (3 July 1934).

[2] S. Taguchi, T. Yamamoto, and A. Sakakura, New grain-oriented silicon steel with high permeability "orientcore HI-B", IEEE Trans. Magn. **10**, 123 (1974).

[3] S. Mishra, C. Därmann, and K. Lücke, On the development of the Goss texture in iron-3% silicon, Acta Metall. **32**, 2185 (1984).

[4] K. I. Arai and K. Ishiyama, Rolled texture and magnetic properties of 3% silicon steel, J. Appl. Phys. **64**, 5352 (1988).

[5] International standard, U.S. Patent No. IEC 60404-2:2008 (1996).

[6] R. Schäfer and S. Schinnerling, Bulk domain analysis in FeSi-crystals, J. Magn. Magn. Mater. **215**, 140 (2000).

[7] S. W. Lee, D. S. Hussey, D. L. Jacobson, C. M. Sim, and M. Arif, Development of the grating phase neutron interferometer at a monochromatic beam line, Nucl. Instrum. Methods Phys. Res., Sect. A **605**, 16 (2009).

[8] S. W. Lee, Y. K. Jun, and O. Y. Kwon, A neutron dark-field imaging experiment with a neutron grating, interferometer at a thermal neutron beam line at HANARO, J. Korean Phys. Soc. **58**, 730 (2011).

[9] E. Calzada, F. Gruenauer, M. Mühlbauer, B. Schillinger, and Michael Schulz, New design for the ANTARES-II facility for neutron imaging at FRM II, Nucl. Instrum. Methods Phys. Res., Sect. A **605**, 50 (2009).

[10] C. Grünzweig *et al.*, Neutron Decoherence Imaging for Visualizing Bulk Magnetic Domain Structures, Phys. Rev. Lett. **101**, 025504 (2008).

[11] C. Grünzweig, C. David, O. Bunk, J. Kohlbrecher, E. Lehmann, Y. W. Lai, R. Schäfer, S. Roth, P. Lejcek, J. Kopecek, and F. Pfeiffer, Visualizing the propagation of volume magnetization in bulk ferromagnetic materials by neutron grating interferometry, J. Appl. Phys. **107**, 09D308 (2010).

[12] C. Grünzweig, C. David, O. Bunk, M. Dierolf, G. Frei, G. Kühne, R. Schäfer, S. Pofahl, H. M. R. Rønnow, and F. Pfeiffer, Bulk magnetic domain structures visualized by neutron dark-field imaging, Appl. Phys. Lett. **93**, 112504 (2008).

[13] I. Manke *et al.*, Three-dimensional imaging of magnetic domains, Nat. Commun. **1**, 125 (2010).

[14] A. P. Kaestner, S. Hartmann, G. Kühne, G. Frei, C. Grünzweig, L. Josic, F. Schmid, and E. H. Lehmann, The ICON beamline—A facility for cold neutron imaging at SINQ, Nucl. Instrum. Methods Phys. Res., Sect. A **659**, 387 (2011).

[15] C. Gruenzweig, G. Frei, E. Lehmann, G. Kühne, and C. David, Highly absorbing gadolinium test device to characterize the performance of neutron imaging detector systems, Rev. Sci. Instrum. **78**, 053708 (2007).

[16] A. Hubert and R. Schaefer, *Magnetic Domains* (Springer, Berlin Heidelberg, 1998).

[17] B. D. Cullity and C. D. Graham, *Introduction to Magnetic Materials* (IEEE Press, Piscataway, 2009).

[18] H. Barkhausen, Two phenomena, discovered with the help of the new amplifiers, Phys. Z. **20**, 401 (1919).

[19] S. Shin, R. Schaefer, and B. C. De Cooman, Grain boundary penetration by lancet domains in Fe-3%Si grain-oriented steel, IEEE Trans. Magn. **46**, 3574 (2010).

[20] M. Pott-Langemeyer, B. Weidenfeller, and W. Riehemann, Measurement and calculation of frequency dependent losses in grain oriented electrical sheets, in *Soft Magnetic Materials* edited by D. Raabe and Stahleisen (Düsseldorf, Germany, 2004), Vol. 1, pp. 227–232.